Tellus (1991), *43A*, 226–234

Dissipation of linear mountain waves over a ridge

By WILLIAM BLUMEN and KEVIN RAEDER, *Department of Astrophysical, Planetary, and Atmospheric Sciences, University of Colorado, Campus Box 391, Boulder, CO 80309 USA*

(Manuscript received 17 May 1990; in final form 12 October 1990)

ABSTRACT

Stationary vertically propagating mountain waves generated by flow over a bell-shaped ridge are considered. Dissipation by momentum diffusion is introduced when the disturbed isentropes become nearly vertical. Momentum diffusion, characterized by a constant eddy diffusion coefficient, partially suppresses the amplitude growth of the wave that is a consequence of conservation of wave-energy density. The propagating wave can continue to grow in amplitude until neutral static stability is achieved. At higher levels, wave overturning could be expected to occur. The present solution is contrasted with the solution over a sinusoid. In the latter case, wave saturation can occur, whereby a constant wave amplitude can be maintained by a balance between exponential growth and dissipative decay. Wave momentum flux and its divergence, calculated from each type of solution, are compared. The results are relevant to the parameterization of wave drag associated with the vertical propagation of internal gravity waves. It is concluded that parameterization schemes that incorporate wave drag by use of a monochromatic wave response need to be modified to include the presence of a spectrum of waves from realistic wave sources, such as orography. It appears that the required modifications are principally quantitative adjustments to eddy diffusion coefficients, which take account of the fact that a saturation wave-amplitude cannot be attained for a unique value of the diffusion coefficient.

1. Introduction

Models of the atmospheric circulation on the planetary scale often reveal westerly zonal winds that are in excess of observed winds in a layer that encompasses the lower stratosphere (Tanaka, 1986) to as high as mesopause levels (Holton, 1982). These authors, as well as others, have investigated the role of induced internal gravity-wave drag on simulations of middle atmospheric zonal circulations. The essential feature of these models is the introduction of a drag force that is intended to simulate the divergence of the vertical flux of horizontal momentum. Reported results appear to indicate that this type of drag mechanism, as contrasted with Rayleigh friction for example, provide significant improvements in the prediction of realistic zonal wind profiles in the middle atmosphere.

At present, all the drag parameterizations that have been incorporated into models appear to be based on the wave-drag mechanism suggested by Lindzen (1981) or variants thereof. A review of these procedures will not be attempted; Schoeberl (1988) has provided a well-balanced critique of the principal features of such parameterization schemes. The basic principle is that vertically propagating internal gravity waves grow in amplitude with height z so as to conserve wave energy density in a compressible atmosphere. At some level z_c determined by the properties of the waves and characteristics of the background flow, isentropes will become vertical. This feature will be evident when $\theta_z = -\theta_{0z}$, where θ denotes the potential temperature associated with the wave disturbance and θ_0 represents the background state. Lindzen suggests that eddy diffusion processes (momentum and heat) will prevent overturning when the wave-amplitude exceeds the value needed to achieve neutral stability at $z = z_c$. Inclusion of eddy diffusion by means of an eddy viscosity coefficient, for example, serves to maintain the wave in a *saturated state*: there is a balance between exponential amplitude growth associated with conservation of wave energy density and exponential decay associated with eddy diffusion. It is shown that this relatively simple model hypothesis may be used to determine a divergence of the vertical flux of horizontal momentum that provides, at least to a first approximation, a reasonably accurate zonal wind reduction in the middle atmosphere, e.g., Holton (1982).

Lindzen's approach provides a viable scheme that can be tested and appropriately modified. One principal limitation, at least in the original formulation, is the consideration of only a monochromatic gravity wave in the determination of wave drag. This may be a suitable approximation if the background flow acts to filter out most of the gravity wave spectrum by reflection at low levels. Schoeberl (1988) has considered the spectrum of gravity waves forced by flow over a ridge, and has maintained saturation by introduction of a convective adjustment scheme. Details will not be reviewed here. Blumen (1990) has also incorporated momentum diffusion to alleviate wave breaking, but only in a limited part of the wave where isentropes are nearly vertical. Blumen's approach is similar to a convective adjustment scheme, and is based on the same model assumptions used in the present study. Comparison with Schoeberl's (1988) work is not attempted, because his numerical results are based on the use of a winter zonal mean wind profile and a standard atmosphere temperature distribution. For present purposes, it is sufficient to note that breaking levels z_c and deceleration of the zonal wind are affected when a spectrum of gravity waves is considered in the wave-drag scheme.

The present study considers uniform flow $\bar{u}$ over a ridge to excite a spectrum of gravity waves. The model, developed in Section 2, is hydrostatic and the earth's rotation is neglected. These assumptions limit the wavelength λ to $2\pi\bar{u}N^{-1} < \lambda < 2\pi\bar{u}f^{-1}$. Use of $\bar{u} \approx 10\ \mathrm{ms}^{-1}$, Brunt-Väisälä frequency $N \approx 10^{-2}\ \mathrm{s}^{-1}$ and Coriolis parameter $f \approx 10^{-4}\ \mathrm{s}^{-1}$ provide lower and upper bounds of about 6×10^3 m and 6×10^5 m. Wave solutions associated with the use of a constant eddy diffusion coefficient are presented in Section 3. The results show that wave saturation, in the sense of Lindzen's hypothesis, does not occur. The wave amplitude will initially be reduced below the critical value needed to achieve neutral stability, but ultimately will grow to a critical amplitude at some higher level $z > z_c$.

The present model results are limited by the use of uniform conditions but, most importantly, the present analytical development exhibits the momentum flux and its divergence, in Section 5, as functions of model parameters in a relatively simple manner. Final remarks follow in Section 6.

2. Anelastic model

The present description of mountain waves will be developed from the linearized system of anelastic equations presented by Ogura and Phillips (1962). This set of equations will be expressed in its simplest form: the disturbances are two-dimensional and hydrostatic with the basic flow and static stability parameter independent of height. The appropriate equations are:

$$\bar{u}\frac{\partial u}{\partial x} = -\frac{\partial \pi}{\partial x} + D\frac{\partial^2 u}{\partial x^2}, \tag{1}$$

$$0 = -\frac{\partial \pi}{\partial z} + g\theta, \tag{2}$$

$$\frac{\partial}{\partial x}\rho_a u + \frac{\partial}{\partial z}\rho_a w = 0, \tag{3}$$

$$\bar{u}\frac{\partial}{\partial x}g\theta + N^2 w = 0, \tag{4}$$

where (x, z) denote the horizontal and vertical coordinates, (u, v) denote the velocity components in the (x, z) direction, $\bar{u}$ is the basic flow, N is the Brunt-Väisälä frequency, g is the acceleration of gravity, $\rho_a = \rho_a(0)\exp(-gz/c^2)$ is the adiabatic density distribution and c^2 is the constant adiabatic sound speed. The quantities (π, θ) are defined as

$$\pi = (p - p_a)/\rho_{a0}, \tag{5a}$$

$$\theta = (T - T_a)/T_{a0}, \tag{5b}$$

which represent pressure and temperature perturbations from the basic adiabatic state and the subscript zero denotes a constant reference value. Momentum diffusion or eddy viscosity is associated with a constant diffusion coefficient D.

Present purposes are served by recasting (3) into the equivalent form

$$\frac{\partial u}{\partial x}+\frac{\partial w}{\partial z}-\frac{g}{c^2}w=0. \tag{6}$$

Momentum diffusion will not be incorporated into the model solution until a state of neutral static stability is attained or nearly attained. In the lower atmosphere, where $D=0$, the model (1–4) is adiabatic and inviscid. The appropriate lower boudary condition is

$$w=\bar{u}\,\partial h/\partial x, \qquad z=0, \tag{7}$$

where $h=h(x)$ represents the ridge profile. The solution aloft, where $D\neq 0$, is yet to be determined. However, the appropriate solution must satisfy the radiation condition as $z\to\infty$.

A relationship between u and w may be obtained from (1), (2), (4) and (6) that takes the form

$$\left[N^2+\bar{u}^2\frac{\partial^2}{\partial z^2}-\bar{u}^2\frac{g}{c^2}\frac{\partial}{\partial z}\right]w=-\bar{u}D\frac{\partial^3 u}{\partial z^3}. \tag{8}$$

It is convenient to represent (u, w) in terms of the streamline displacement δ as

$$u=-\bar{u}\left(\frac{\partial\delta}{\partial z}-\frac{g}{c^2}\delta\right), \tag{9a}$$

$$w=\bar{u}\frac{\partial\delta}{\partial x}. \tag{9b}$$

This representation satisfies the continuity eq. (6). Substitution of (9a, b) into (8) yields the fourth-order partial differential equation

$$D\frac{\partial^4\delta}{\partial z^4}-D\frac{g}{c^2}\frac{\partial^3\delta}{\partial z^3}-\bar{u}\left(\frac{\partial^2}{\partial z^2}-\frac{g}{c^2}\frac{\partial}{\partial z}+l^2\right)\frac{\partial\delta}{\partial x}=0, \tag{10}$$

where $l=N/\bar{u}$. This eq. (10) may be cast into non-dimensional form by means of $\delta'=l\delta$, $z'=lz$ and $x'=x/a$, where a is the characteristic half-width of the ridge profile. For the present model, the characteristic parameter values are $l\approx 10^{-3}\,\mathrm{m}^{-1}$ and $a\approx 20-30\times 10^3$ m. Hereafter, the prime notation will be omitted from nondimensional variables. The governing equation (10) expressed in nondimensional form, is

$$\gamma\frac{\partial^4\delta}{\partial z^4}-\gamma\varepsilon\frac{\partial^3\delta}{\partial z^3}-\left[\frac{\partial^2}{\partial z^2}-\varepsilon\frac{\partial}{\partial z}+1\right]\frac{\partial\delta}{\partial x}=0, \tag{11}$$

where

$$\gamma=al^2D/\bar{u}, \tag{12a}$$

$$\varepsilon=(g/c^2)/l. \tag{12b}$$

The parameter ε satisfies $\varepsilon\sim(10/10^5)/10^{-3}\sim 10^{-1}$, and the parameter γ satisfies $\gamma\leqslant 10^{-1}$ if $D\leqslant 10^3\,\mathrm{m^2\,s^{-1}}$ with $a\approx 25\times 10^3$ m and $\bar{u}\approx 25\,\mathrm{ms^{-1}}$. These parameters (γ, ε) provide measures of the relative importance, respectively, of momentum diffusion and atmospheric compressibility.

The basic eq. (11) may be simplified by introduction of the transformation

$$\delta=e^{\varepsilon z/2}\,\Delta(z), \tag{13}$$

and the neglect of all terms multiplied by products ε^2, $\varepsilon\gamma$, ... The reduced form of (11) becomes

$$\gamma\frac{\partial^4\Delta}{\partial z^4}-\left(\frac{\partial^2}{\partial z^2}+1\right)\frac{\partial\Delta}{\partial x}=0. \tag{14}$$

The inviscid wave equation is recovered by setting $\gamma=0$. The solution may be obtained by first taking the Fourier transform of (14) to obtain

$$\left(\frac{i\gamma}{k}\frac{\mathrm{d}^4}{\mathrm{d}z^4}+\frac{\mathrm{d}^2}{\mathrm{d}z^2}+1\right)\hat{\Delta}=0, \tag{15}$$

where $\hat{\Delta}$ represents the transform of Δ and k, the horizontal wave number, is non-dimensional. The four independent solutions may be found by substituting $\hat{\Delta}\propto\exp imz$ into (15), and then solving the quartic equation for m. The algebra will not be displayed here. It is only necessary to note that two solutions essentially represent a balance between the first two terms of (15). The physically acceptable solution of these has a relatively short penetration depth above the level where $\gamma\neq 0$, and will therefore not be considered. The remaining two solutions represent relatively small viscous modifications to the inviscid solution. The appropriate root that satisfies the radiation condition is provided by

$$m_L \approx 1 + \frac{1}{2}\frac{i\gamma}{k}. \tag{16}$$

This expression (16) is, in essence, Lindzen's (1981) result taking account of the anelastic approximation used in the present study. Lindzen's approximation is compared to the exact root of (15) in Fig. 1. The approximate root m_L is reasonably accurate for $\gamma/k < 0.3$.

There is an abrupt transition at z_c from the region below where $\gamma = 0$ to the region above where $\gamma \neq 0$. Consequently, a vertically propagating wave in $z < z_c$ will undergo partial reflection at $z = z_c$. The reflection coefficient $|R|$ the manitude of the ratio of the reflected to transmitted wave, may be determined by the requirement that the pressure and streamline displacement be continuous at z_c. This evaluation yields $|R| \approx |\varepsilon/2 - \gamma/k| < 10^{-1}$, for the parameter values presented in Fig. 2. The reflected wave may be neglected, and the complete solution for δ (13) may now be expressed as

$$\delta = \mathrm{Re}\, e^{(\varepsilon/2+i)z} \int_0^\infty F(k)\, e^{ikx}\, dk,$$

$$z \leqslant z_c, \tag{17}$$

$$\delta = \mathrm{Re}\, e^{(\varepsilon/2+i)z} \int_0^\infty F(k)\, e^{-(\gamma/2k)(z-z_c)} e^{ikx}\, dk,$$

$$z \geqslant z_c, \tag{18}$$

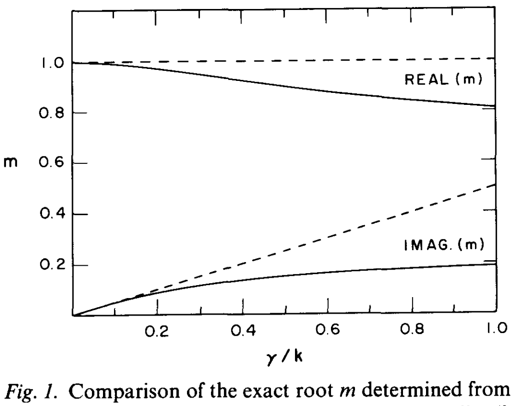

Fig. 1. Comparison of the exact root m determined from the quartic equation (15) (solid) with its small γ/k approximation m_L (dashed).

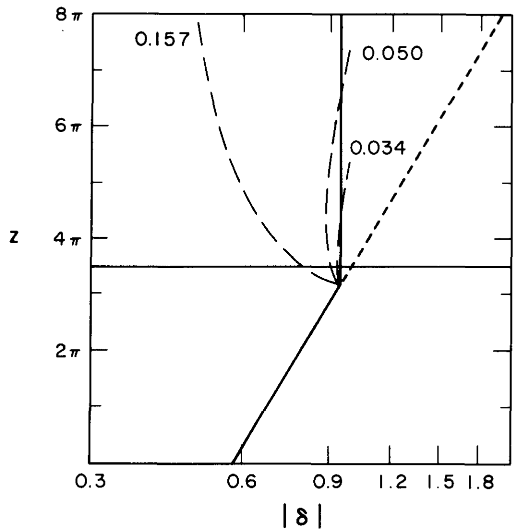

Fig. 2. Wave-amplitudes $|\delta|$ for the values of γ shown (long-dashed) compared with Lindzen's (saturated) wave-amplitude (solid), which is evaluated by means of (31) with $\gamma = 0.157$ and $k_0 = 1$. The wave-amplitude in an inviscid atmosphere is shown for reference (short-dashed). The dissipation is introduced slightly below the first overturning level (horizontal line). The dashed curves terminate at levels where neutral stability is attained.

where z_c is the level at which momentum diffusion is introduced, and F is the Fourier transform of $h(x)$.

3. Solution

The solution provided by (18) satisfies the radiation condition when $\gamma = 0$. The lower boundary condition (7) may be expressed as

$$\delta = h(x), \qquad z = 0, \tag{19}$$

using (9b). The ridge will be represented by the bell-shaped profile

$$h(x) = h_0/(1 + x^2), \tag{20}$$

where h_0 is the nondimensional crest height and x is measured in half-widths of the ridge. The Fourier transform of (20) is

$$F(k) = h_0 e^{-k}. \tag{21}$$

Insertion of (21) into (17) yields the classical Queney (1948) solution

$$\delta = \frac{h_0 e^{\varepsilon z/2}}{1+x^2}(\cos z - x \sin z). \tag{22}$$

Substitution of (21) into (18) provides a Laplace transform integral evaluated in Erdélyi et al. [1954, p. 146 (25)], and expressed as

$$\delta = \mathrm{Re}\, e^{(\varepsilon/2+i)z} h_0 \left\{ \left[\frac{2\gamma(z-z_c)}{1-ix} \right]^{1/2} \times K_1([2\gamma(z-z_c)(1-ix)]^{1/2}) \right\}, \qquad z \geqslant z_c, \tag{23}$$

where (γ, ε) are defined by (12a, b) and $K_1(y)$ denotes the Modified Bessel Function of complex argument. It may be noted that

$$K_1(y) \to y^{-1} \quad \text{as} \quad y \to 0, \tag{24}$$

(Olver, 1964; Subsection 9.6.9). Consequently, (23) reduces to (22) as $z \to z_c$.

The asymptotic expression for K_1, provided by Olver (1964; Subsection 9.7.2), is given by

$$K_1(y) = (\pi/2y)^{1/2} e^{-y}(1 + 3/8y + \cdots). \tag{25}$$

Evaluating of (23) by means of (25) yields, to leading order,

$$\begin{aligned} \delta \approx \left(\frac{\pi}{2}\right)^{1/2} & \frac{h_0}{1+x^2} [2\gamma(z-z_c)(1+x^2)]^{1/4} \\ & \times \exp\left\{ \frac{\varepsilon z}{2} - [2\gamma(z-z_c)]^{1/2} \alpha \right\} \\ & \times \{(\alpha\lambda - \beta\mu)\cos(z - [2\gamma(z-z_c)]^{1/2}\beta) \\ & + (\alpha\mu + \beta\lambda)\sin(z - [2\gamma(z-z_c)]^{1/2}\beta)\}, \end{aligned} \tag{26}$$

where

$$\alpha = \left[\frac{1}{2}(1+x^2)^{1/2} + \frac{1}{2} \right]^{1/2}, \tag{27a}$$

$$\beta = \left[\frac{1}{2}(1+x^2)^{1/2} - \frac{1}{2} \right]^{1/2}, \tag{27b}$$

$$\lambda = \left[\frac{1}{2}(1+x^2)^{1/4} + \frac{\alpha}{2} \right]^{1/2}, \tag{27c}$$

$$\mu = \left[\frac{1}{2}(1+x^2)^{1/4} - \frac{\alpha}{2} \right]^{1/2}. \tag{27d}$$

4. Discussion

The numerical evaluation of (23) is provided in Section 5. Here properties of the asymptotic solution, provided by (26) are contrasted with solutions presented by Lindzen (1981).

Lindzen considered a monochromatic wave response, which may be derived by setting F in (18) equal to a delta function with argument $k - k_0$. The solution takes the relatively simple form

$$\delta \propto e^{1/2(\varepsilon - \gamma/k_0)z} \cos(k_0 x + z), \qquad z \geqslant z_c. \tag{28}$$

It may be noted from (4) and (9b) that $\delta \propto \theta$, where θ is defined by (5b). At some upper level exponential amplitude growth, associated with atmospheric compressibility ($\varepsilon \neq 0$), can cause the isentropes to become vertical, a state of neutral static stability. Lindzen determines the magnitude of the diffusion coefficient that keeps the wave in this saturated state, i.e., $\varepsilon - \gamma/k_0 = 0$ in (28). Use of (12a, b) yields the condition

$$D = k_0(g/c^2)\,\bar{u}/l^3, \tag{29}$$

where k_0 is now expressed as a *dimensional* quantity. Evaluation of eq. (29) using $k_0 \approx 10^{-4}\ \mathrm{m}^{-1}$, $g \approx 10\ \mathrm{ms}^{-2}$, $c^2 \approx 10^5\ \mathrm{m}^2\,\mathrm{s}^{-2}$, $\bar{u} \approx 25\ \mathrm{ms}^{-1}$, and $l \approx 10^{-3}\ \mathrm{m}^{-1}$, yields $D \approx 250\ \mathrm{m}^2\,\mathrm{s}^{-1}$. This value is the same order as the magnitude of the eddy coefficient determined by Lindzen although different parameter values are used.

Although Lindzen's solution provides a conceptual framework in which to explain the saturation of a vertically propagating gravity wave, the restriction to a monochromatic wave places a restriction on the applicability of his result. Most forcing mechanisms, such as the earth's orography initiate a spectrum of motions. It is possible, that wave reflection in the lower atmosphere may lead to a dominant monochromatic wave in the upper atmosphere and a physically interesting situation in which Lindzen's saturation mechanism is valid. However, if a spectrum of waves is present above z_c, then the solution provided by either (23) or (26) cannot reach a saturated state: exponential growth associated with compressibility cannot be balanced by momentum diffusion since the latter process is associated with an exponential decay that depends on $z^{1/2}$, at least for the forcing mechanism provided by (20).

5. Model characteristics

The effect of the lower boundary condition on solutions of Lindzen's model will now be explored. The principal effect, the difference in viscous decay rates, is clearly evident in the comparison between (26) and (28). The amplitudes $|\delta|$ are shown as functions of height z in Fig. 2. The height at which neutral stability is first attained is determined as in Blumen (1988, Section 5) and Raeder (1990). The ridge crest is $h_0 = 0.577$ (577 m), and the inviscid wave would reach a state of neutral stability, the "breaking-level", at the height delineated by the horizontal line in Fig. 2. The wave-amplitude growth in an inviscid atmosphere that proceeds along the short dashed line is shown for reference. Saturation, for a monochromatic wave is denoted by the solid vertical line associated with $\gamma = 0.157$. In contrast, the solution (23), associated with $\gamma = 0.157$ (dashed) does not reach a breaking level in the vertical domain displayed in Fig. 3. The other dashed curves, representing the solutions for $\gamma = 0.034$ and $\gamma = 0.050$ reach breaking levels, respectively, within one and two vertical wavelengths above the inviscid breaking level. It may be noted that the most significant contribution to the integral (18), with $F(k)$ provided by (21), occurs when $\gamma/k \sim [2\gamma/(z - z_c)]^{1/2}$. The con-

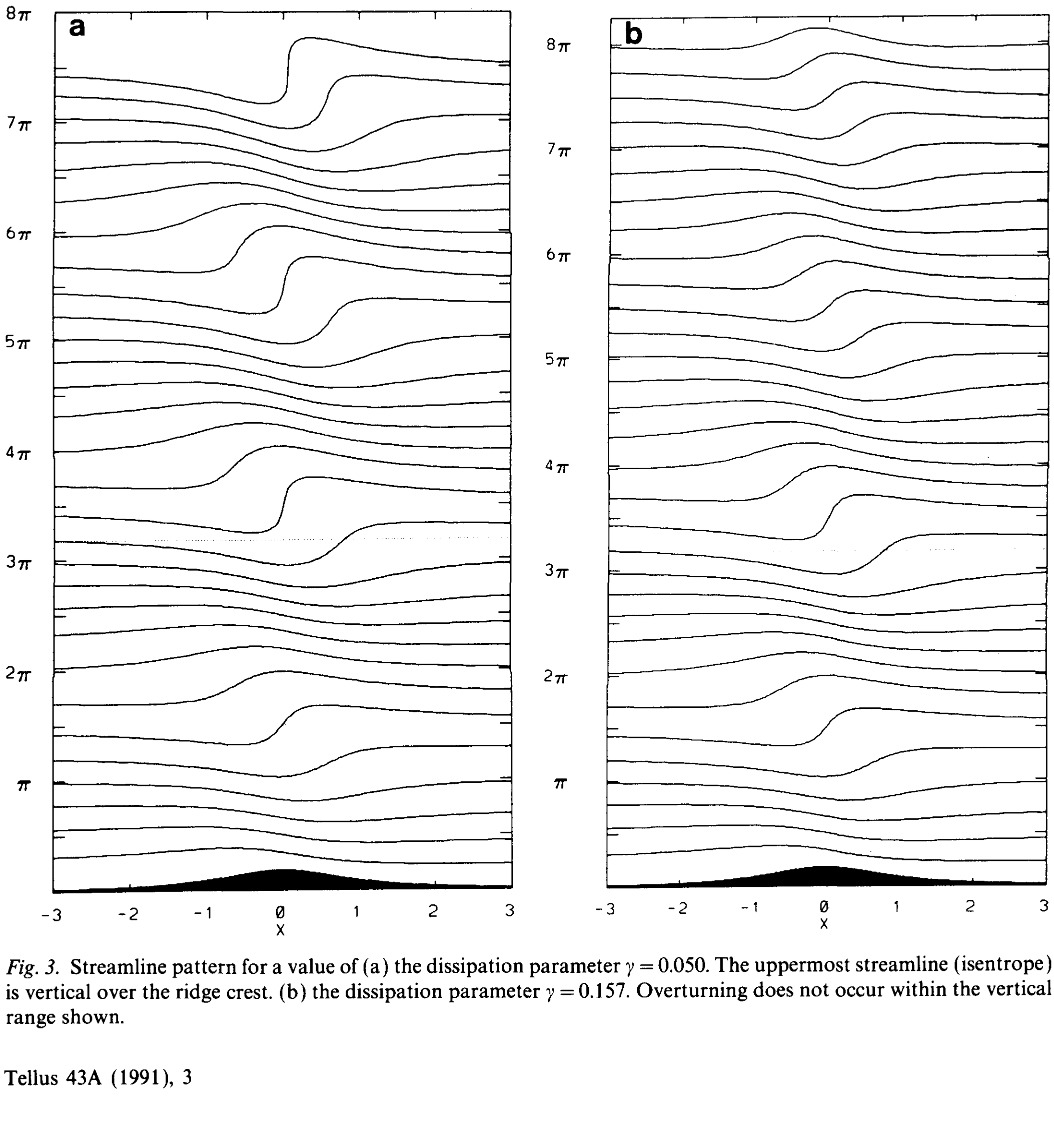

Fig. 3. Streamline pattern for a value of (a) the dissipation parameter $\gamma = 0.050$. The uppermost streamline (isentrope) is vertical over the ridge crest. (b) the dissipation parameter $\gamma = 0.157$. Overturning does not occur within the vertical range shown.

straint $\gamma/k < 0.3$, that is associated with the use of (16), is satisfied by the values of γ appearing in Fig. 2 when $z - z_c > \pi$.

There are some minor features, such as an increase in the vertical wavelength and an x-dependent phase shift, that are evident in the asymptotic representation (26). The streamline patterns, displayed in Figs. 3a and 3b show that these effects are relatively unimportant, particularly in the context of the simplifications associated with this model, e.g., uniform background state.

Yet even a small amount of dissipation can affect the motion field in a significant manner. As long as the flow is essentially inviscid and linear (and there are no critical levels in the flow) the vertical flux of horizontal momentum is constant with height (Eliassen and Palm, 1961). In these regions, the background flow is unaffected by the waves. In the present model, however, there is divergence of the vertical flux of horizontal momentum associated with the wave solutions (23) and (28).

The vertical flux of horizontal momentum for a gravity wave can be represented as $F = \rho_a \overline{uw}^x$, where $\rho_a(z)$ is the background adiabatic density distribution, and the heavy overbar indicates an average over the domain of x appropriate to the orography

$$\overline{(\;)}^x \equiv \frac{1}{2L} \int_{-\infty}^{\infty} (\;)\,\mathrm{d}x, \tag{30}$$

where $2L$ is a characteristic mountain width. The horizontal and vertical velocities are determined from (9a, b) using (23). The flux F_s has also been determined when the lower boundary is a sinusoid, $h = h_s \sin k_0 x$, characterized by amplitude h_s and wavenumber k_0. The constant inviscid fluxes associated with the bell-shaped profile (20) and the sinusoid are equated. The flux F_s in the dissipative region ($z > z_0$) is determined from (9a, b) and

$$\delta = \frac{h_s}{2} \exp\left[\frac{\varepsilon}{2} z - \frac{\gamma}{2k_0}(z - z_c)\right] \times \sin(k_0 x + z). \tag{31}$$

The corresponding value of the flux is

$$F_s = -\frac{\pi}{16} h_s^2 \exp\left[-\frac{\gamma}{k_0}(z - z_c)\right]. \tag{32}$$

The distribution of F, associated with the ridge (20), is determined by numerical evaluation.

The fluxes associated with the sinusoidal and isolated ridges are displayed as functions of height in Fig. 4. The fluxes are constant up to the dissipation height z_c, taken to be slightly below the height where neutral stability occurs. The termination levels are the breaking levels associated with $h_0 = 0.577$, $\varepsilon = 0.1$ and γ.

Wave-induced accelerations of the zonal-mean flow may be evaluated by (Lindzen, 1981)

$$X = -\frac{1}{\rho_a(z)} \frac{\partial F}{\partial z}, \tag{33}$$

where $F = \rho_a(z)\,\overline{uw}^x$. Results for the three solutions in Fig. 4 are shown in Fig. 5. Relatively large vertical gradients of F, associated with the isolated ridge solution, occur just above the inviscid solution (Fig. 4). This feature is reflected in the relatively larger low-level accelerations in Fig. 5. Otherwise, the accelerations exhibit similar orders of magnitude, although the ridge solution is only valid up to the level where its overturning amplitude is reached.

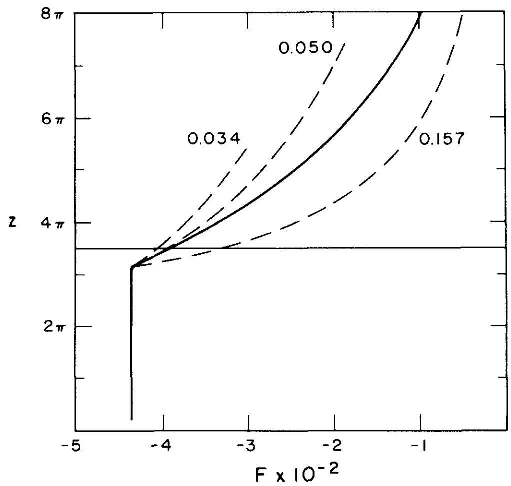

Fig. 4. Vertical flux of horizontal momentum F for values of γ as shown. Lindzen's flux (saturated wave, see Fig. 2) is shown for comparison (solid). The flux has units of $\rho_a(0)\, U^2/al$. For $\rho_a(0) = 1.2$ kg/m^3, $U = 20$ m/s, $a = 20$ km, and $l \equiv 10^{-3}$ m^{-1}, $F = -1 \times 10^{-2}$ represents a flux of -2.4×10^{-1} N/m^2.

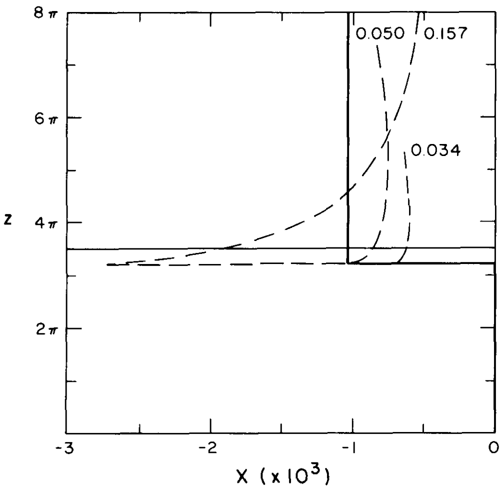

Fig. 5. As in Fig. 4, but for zonal-flow deceleration for values of γ as shown. $X = -1 \times 10^3$ represents an deceleration of 20 ms^{-1} day^{-1}.

6. Remarks

The present study is intended to examine the saturation hypothesis, presented by Lindzen (1981), when a spectrum of waves is present. The discrete breaking levels associated with flow over a ridge, found earlier by Schoeberl (1988) and Blumen (1988) distinguish the present solutions from monochromatic waves forced by a sinusoid. The principal result, however, is the presentation of analytical solutions that exhibit the interplay between wave-amplitude growth that preserves the constant energy density and momentum diffusion that seeks to achieve a saturated state-no growth. The solutions (23 or 26) show that the rate of wave-amplitude growth cannot be balanced by dissipation over a layer depth: dissipation can only retard the inexorable growth to an amplitude at which neutral stability is achieved. For relatively large values of the eddy diffusion coefficient this retardation can delay the growth to a breaking level z over several vertical wavelengths, and neglected physical processes may become important, e.g., zonal wind variations. Similarly, (26) shows that the breaking level will also be raised if a lower ridge crest h_0 is specified. Consequently, predictions of breaking levels, based on the present results, are not proposed. The results do show that the Lindzen parameterization scheme may provide a gravity-wave drag in large-scale model simulations even when a spectrum of waves is considered. The modifications suggested by Figs. 3–5 are the reevaluation of eddy diffusion coefficients that account for gravity-wave sources, such as flow over orography, and the need to limit wave-breaking at even higher altitudes where low-level attenuation is not sufficient to completely suppress wave-amplitude growth.

7. Acknowledgements

Support for this study has been provided by the National Science Foundation under grants ATM 86-08333 and ATM 88-20164. Computations have been carried out on the Pyramid 90X super mini-computer in the University of Colorado Center for Atmospheric Theory and Analysis. We thank Jeff de La Beaujardiere for providing, for our use, the subroutine to calculate the modified Bessel function.

REFERENCES

Blumen, W. 1988. Wave breaking in a compressible atmosphere. *Geophys. Astrophys. Fluid Dynamics 43*, 311–332.

Blumen, W. 1990. Finite-amplitude mountain waves in a compressible atmosphere including the effects of dissipation. *Geophys. Astrophys. Fluid Dynamics 52*, 89–104.

Eliassen, A. and Palm, E. 1961. On the transfer of energy in stationary mountain waves. *Geofys. Publ. Oslo 22(3)*, 1–23.

Erdélyi, A., Magnus, W., Oberhettinger, F. and Tricomi, F. G. 1954. *Tables of integral transforms, vol. 1.* McGraw-Hill, 391 pp.

Holton, J. R. 1982. The role of gravity wave induced drag and diffusion in the momentum budget of the mesosphere. *J. Atmos. Sci. 39*, 791–799.

Lindzen, R. S. 1981. Turbulence and stress owing the gravity wave and tidal breakdown. *J. Geophys. Res. C10*, 9707–9714.

Ogura, Y. and Phillips, N. A. 1962. Scale analysis of deep and shallow convection in the atmosphere. *J. Atmos. Sci. 19*, 173–179.

Olver, F. W. J. 1964. Bessel functions of integral order. Handbook of mathematical functions. (Eds. Abramowitz, M. and Stegun, I. A.), *Nat. Bur. Stnds.* 355–436.

Queney, P. 1948. The problem of air flow over mountains: A summary of theoretical studies. *Bull. Amer. Meteor. Soc. 29*, 16–26.

Raeder, K. 1990. *Dissipation of linear gravity waves generated by an isolated ridge.* Masters Thesis, University of Colorado, 52 pp.

Schoeberl, M. R. 1988. A model of stationary gravity wave breakdown with convective adjustment. *J. Atmos. Sci. 45*, 980–992.

Tanaka, H. 1986. A slowly varying model of the lower stratospheric zonal wind minimum induced by mesoscale mountain wave breakdown. *J. Atmos. Sci. 43*, 1881–1892.